Ferroelectrics

ISSN: 0015-0193 (Print) 1563-5112 (Online) Journal homepage: http://www.tandfonline.com/loi/gfer20

Electron Spectroscopy and the Electronic Structure of $KNbO_3$: First Principle Calculations

S. Simsek , H. Koc , V. A. Trepakov , A. M. Mamedov & E. Ozbay

To cite this article: S. Simsek , H. Koc , V. A. Trepakov , A. M. Mamedov & E. Ozbay (2014) Electron Spectroscopy and the Electronic Structure of $KNbO_3$: First Principle Calculations, Ferroelectrics, 461:1, 99-105, DOI: 10.1080/00150193.2014.889998

To link to this article: http://dx.doi.org/10.1080/00150193.2014.889998

Ferroelectrics, 461:99–105, 2014

ISSN: 0015-0193 print / 1563-5112 online
DOI: 10.1080/00150193.2014.889998

Taylor & Francis
Taylor & Francis Group

Electron Spectroscopy and the Electronic Structure of $KNbO_3$: First Principle Calculations

S. SIMSEK,[1] H. KOC,[2] V. A. TREPAKOV,[3] A. M. MAMEDOV,[4,*] AND E. OZBAY[4]

[1]Hakkari University, Turkey
[2]Siirt University, Turkey
[3]Institute of Physics ASCR, Czech Republic
[4]Bilkent University, Nanotechnology Research Center, Turkey

The electronic structures of $KNbO_3$ were calculated within the density functional theory, and their evolution was analyzed as the crystal-field symmetry changes from cubic to rhombohedral via tetragonal phase. We carried out electron-energy loss spectroscopy experiments by using synchrotron radiation and compared the results with the theoretical spectra calculated within Density Functional Theory. The dominant role of the NbO_6 octahedra in the formation of the energy spectra of $KNbO_3$ compound was demonstrated. The anomalous behavior of plasmons in ferroelectrics was exhibited by the function representing the characteristic energy loss in the region of phase transition.

Keywords $KNbO_3$; electron energy loss; plasmon

Introduction

Over the past decades, electron energy loss (EEL) spectroscopy has developed into a major tool for the characterization of nonlinear structures and electronic structure of materials. Most of these studies focus on the ionization edges, where the position of the edges and their intensity provide a quantitative measure of the composition [1]. The low-loss energy region of the EEL spectrum (<50 eV) can also provide information on the composition and electronic structure, as well as optical properties [1, 2], although it has not found as wide an application as the energy-loss near-edge structure. In this low-loss region, interband transitions and plasmon losses are observed.

The plasmons hold a unique position among the quasiparticles in solids because of their special features. The spectra of plasmons are described by the functions $-\mathrm{Im}\varepsilon^{-1}$ (volume plasmons) and $-\mathrm{Im}(\varepsilon+1)^{-1}$ (surface plasmons). Experimentally, they are determined by measuring the characteristic electron energy losses (EEL) [2]. In general, the half-width of the principal W peak typically exceeds 4.0 eV. The intensity of the W peak critically depends on the orientation of the sample and the energy of the electron beam, their resolution being not finer than 1.0 eV. This severely hampers the determination of true plasmon spectra. Of great interest, in this connection, is a calculation procedure in which the experimental data

Received September 2, 2013; in final form November 5, 2013.
*Corresponding author. E-mail: mamedov@bilkent.edu.tr

on the reflection spectra and the Kramers-Kronig integral relations are used to determine the plasmon spectra [3].

The aim of the present paper is to apply Density Functional Theory (DFT) band structure calculations of the electronic structure, dielectric functions, and spectra of plasmons of both types to a wide variety of $KNbO_3$ in order to explore how low-loss EEL spectra can be predicted.

Our paper is organized as follows. In section 2, we describe the methodology, structure, and computational details. In sections 3–4, we illustrate the validity of the formalism by applying methodology and theory to $KNbO_3$ ferroelectrics.

Computational Details

The optical properties of ABO_3 type compounds were theoretically studied by means of first principles calculations in the framework of density functional theory and based on the local density approximation (LDA) as implemented in the ABINIT code [4, 5]. The self-consistent norm-conserving pseudopotentials are generated using the Troullier-Martiens scheme, which for the $KNbO_3$, include the semicore s and p states of the K- and Nb- atoms (see Table 1) [6] which is included in the Perdew-Wang [7] scheme as parameterized by Ceperly and Alder [8]. For the calculations, the wave functions were expanded in plane waves up to a kinetic-energy cutoff of 40 Ha (tetragonal and rhombohedral $KNbO_3$). The level of accuracy for the Kohn-Sham eigenvalues and eigenvectors is required to calculate the response function. The Brillouin zone was sampled using an $8 \times 8 \times 8$ the Monkhorst-Pack [9] mesh of special k points. The coordinates of $KNbO_3$ [10, 11] are reported in Table 1. All the calculations of $KNbO_3$ have been used with experimental lattice constants and atomic positions. The lattice constants and atomic positions are given in Table 1. The coordinates of the other atoms can easily be obtained by using the symmetry operations of the space groups. These parameters were necessary to obtain converged results of the optical properties.

Table 1
Atomic position and lattice parameters of $KNbO_3$ [10, 11, 20]

Crystals	Symmetry Class	Lattice Parameters [Å]	Atoms, WPa	Position
$KNbO_3$	$m\bar{3}m$	$a = b = c = 4.0214$	K(1a)	(0.0, 0.0, 0.0)
			Nb(1b)	(0.5, 0.5, 0.5)
			O(3c)	(0.5, 0.5, 0.0)
$KNbO_3$	4mm	$a = b = 3.9970$	K(1a)	(0.0, 0.0, 0.023)
		$c = 4.0630$	Nb(1b)	(0.5, 0.5, 0.5)
			O1(1b)	(0.5, 0.5, 0.04)
			O2(2c)	(0.5, 0.0, 0.542)
$KNbO_3$	3m	$a = b = c = 4.016$	K	(0.0112, 0.0112, 0.0112)
			Nb	(0.5, 0.5, 0.5)
			O1	(0.5295, 0.5295, 0.0308)
			O2	(0.5295, 0.0308, 0.5295)

Electronic Structure of the Valence and Conductions Bands

In this section, we describe the evolution of the electronic structure of $KNbO_3$ in the structural and ferroelectric phase transitions in relation with the evolution of the symmetry of the crystal field. The results from vacuum ultraviolet (VUV) reflectivity experiments are reported in the literature for some ABO_3 compounds [12–19]. We furthermore give a comparison of the theoretical band structure of the valence and conduction bands in various phases. Last, we report our results for the theoretical energy gap, and the energy gap values determined experimentally. Since ABO_3 ferroelectrics have been widely studied [12–19] we show in detail only the calculated band structures for $KNbO_3$ in different phases. The dispersion of the energy of the valence bands for the cubic (C), tetragonal (T) and rhombohedral (R) phases at the equilibrium lattice parameters are reported in Fig. 1. The top of the valence band is located at the R point in the cubic and tetragonal phases, and in the Z point in the rhombohedral phase. The DOS reported for all phases in Fig. 1(a)–(c) show a much higher density of states at and near the top of the valence bands. The valence bandwidth decreases by 0.3 eV between the different crystal fields, from 5.6 eV in the cubic phase to 4.3 eV in the rhombohedral phase. The bandwidth of the tetragonal phase is closer to the width of the cubic phase than to the rhombohedral one.

As we stated hereinabove, the electronic band structure of paraelectric cubic $KNbO_3$ along the symmetry lines of the cubic Brillouin zone is shown on Fig. 1(a). Let us now describe the electronic band structure of the $KNbO_3$ in more detail. It is clear that the indirect bad gap appears between the topmost valence band and at the R point and at the bottom of conduction band at the Γ point. The overall profile of our band structure is qualitatively like the band structure obtained by previous studies [13, 14], where the same compound [14] was investigated in the cubic and tetragonal phases. It is observed that the conduction band minimum goes from the Γ point through Δ to the X point and always remains nearly flat in agreement with previous studies [14, 15, 18]. The calculated indirect band gap (R-Γ) is equal to 1.54 eV while the smallest direct band gap (Γ_V-Γ_C) is 2.51 eV. These calculated values are smaller than the experimental value of 3.1 eV for the indirect gap [16]. The origin of this discrepancy could be the use of DFT, which generally underestimates the band gap in semiconductors and insulators [3]. The band with the lowest energy in Fig. 1, lying between -16.0 eV and -17.0 eV, correspond to a very large extent, to O 2*s* states. The nine valence bands between -5.9 eV and the Fermi level (zero) are mainly due to the oxygen O 2*p* states hybridized with Nb 4*d* states. These nine valence bands are split into triple and double degenerate levels at the Γ point (Γ_{15},Γ_{25}, Γ_{25}) separated by energies of 1.64 eV (Γ_{15}-Γ_{25}), of 0.3 eV (Γ_{25}, Γ_{15}), and of 1.94 eV (Γ_{15}-Γ_{25}) due to the crystal field and electrostatic interaction between mainly O 2*p* and Nb 4*d* orbitals. In the conduction band, the one two triply (Γ_{12}) degenerate levels represents Nb 4*d* t_{2g} and Nb e_g orbitals separated by energy of 4.2 eV. The topmost valence bands are the oxygen $2p_x$, $2p_y$ states while the lowest valence bands are formed by the hybridization of Nb 4*d* e_g and O $2p_z$ states. In the conduction band region, the first conduction band from approximately 1.59 eV above the Fermi level to 5.6 eV arises from predominantly Nb t_{2g} states with small O 2*p* mixing. The bands in the conduction band that are shown in Fig. 1 belong to Nb 4*d* e_g states. In additions, some electrons from Nb 4*d* transform into the valence band and take part in the interaction between Nb and O. This implies that there is hybridization between Nb 4*d* and O 2*p*.

The agreement between our density of states (DOS) and the experimental spectrum is good [12–19]. The dispersion curve of the conduction bands at the theoretical equilibrium lattice parameters are reported in Fig. 1(a)–(c). The bottom of the conduction band is found

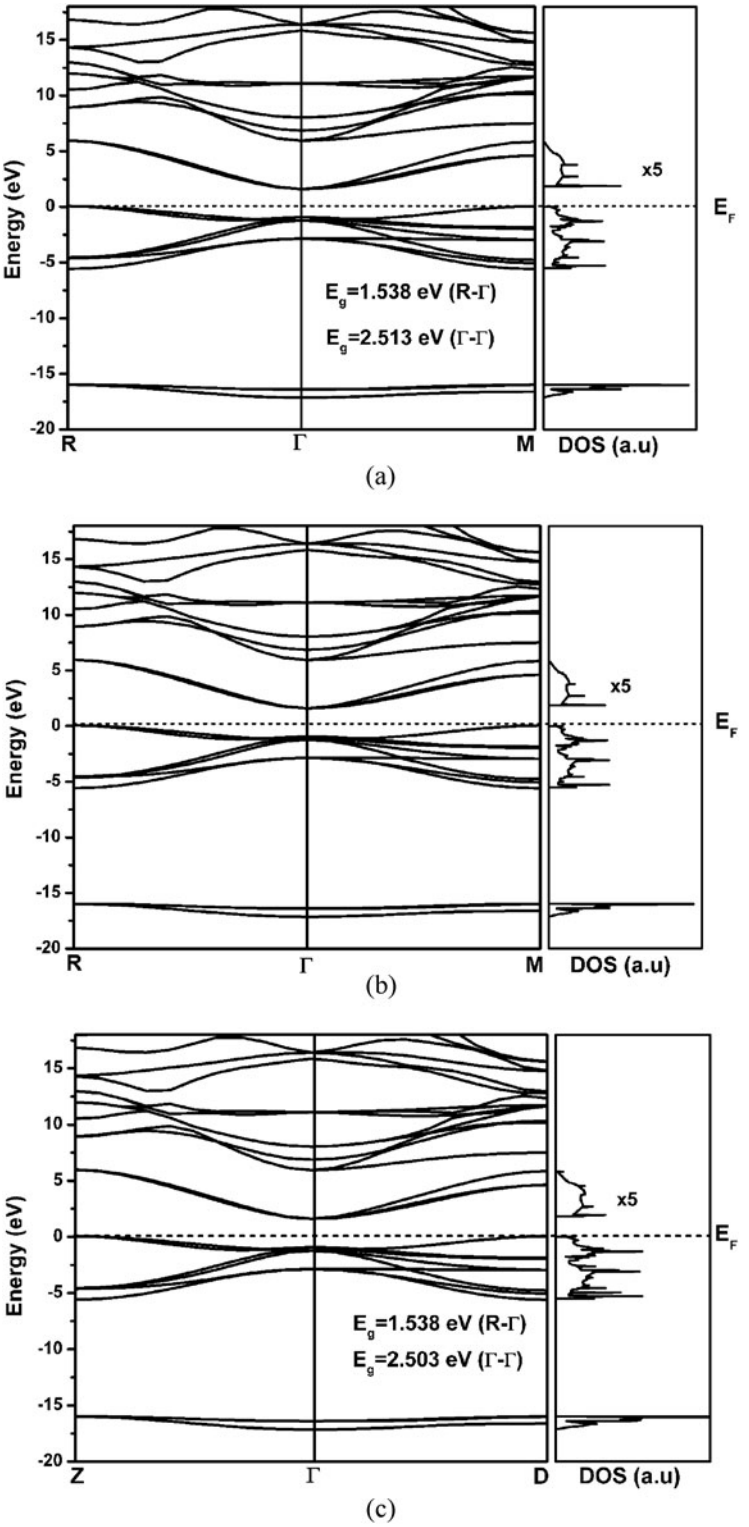

Figure 1. Electronic band structure and DOS of $KNbO_3$, cubic (a), tetragonal (b), rhombohedral (c).

Table 2
Theoretical and experimental data of plasmon energies and energy features of -Imε^{-1} for $KNbO_3$

	Exp	Exp	Theory	Exp[12]	Theoretical
Material	E_p [eV]	E_s [eV *]	E_p [eV]	-Imε^{-1}	-Imε^{-1}
$KNbO_3$/Cubic	—	—	21.8	—	6.5, 15.0, 22.6, 28.1, 41.5
$KNbO_3$/Tetragonal	24.0	17.0	22.0	7.1, 14.0, 23.2, 29.5	6.4, 14.9, 22.5, 28.0, 41.0
$KNbO_3$/Rhombohedral	—	—	21.9	—	6.4, 14.9, 22.5, 28.1, 41.4

to be at the Γ point for all phases. The first conduction bands are found to have an e_g character at the Γ point in the cubic phase (Fig. 1). At higher energy, conduction bands have a_{1g} or t_{2g} character at the R and Γ points. The gap in the conduction band has a minimum of 1.3 eV at Γ point. The fundamental gap of $KNbO_3$ single crystal has been measured in the cubic and tetragonal phases [12]. More precisely, VUV spectroscopy has been performed in reflectivity in the 1.0–35.0 eV range, and the absorption spectrum has been deduced from a Kramers-Kronig analysis [15]. The band gap obtained from a fit of the low absorption is found to be of 2.86 eV. However, EEL spectroscopy experiments a large momentum transfer [17], give a gap value of about 2.9 eV. Our fitted value for E_g amounted to 2.45 eV in the cubic phase of $KNbO_3$. We have also calculated the minimum and direct LDA band gap energy at the theoretical lattice parameters (Table 1). Within the accuracy of our calculations, the values of the direct and indirect band gap are within 2.35 eV of each other in all phases except the rhombohedral one, where the minimum gap is 1.5 eV smaller than the first direct gap. Our results are in a good agreement with the previous calculation [14, 17] performed at the experimental lattice parameters, with the exception of the rhombohedral phase (Table 2).

Energy Loss Spectroscopy

In this section, we first apply the theoretical framework defined in section 3 and report our theoretical EEL spectra. Valence EEL spectroscopy experiments have previously been performed in transmission at a large momentum transfer q [1] and also in the reflection [1, 12]. In this work, we have performed very low q and VUV reflectivity [12–14] experiments and compared them with the theoretical results. In Fig. 2, we report the dielectric functions (real and imaginary parts, and Imε^{-1}) for $KNbO_3$ in three phases: cubic, tetragonal, and rhombohedral, calculated in LDA. Three regions can be distinguished. First, we observe that the valence excitation region extends up to 15.0 eV. The form of the structure and the shape of ε_2 for the investigated crystal are determinate by the positions of the critical state density points. The similarity between the ε_2 for all the modifications of $KNbO_3$ in the region up to 14.0 eV points to a substantial role of NbO_6 octahedra in the formation of the band structure. This means that the NbO_6 octahedra determine the lowest limit of the conduction band and the upper valence band. These bands are similar for many ABO_3 compounds, since the d-orbitals of the transition metals and the *p*-orbitals of oxygen, which are joined in each octahedron, yield the main contribution to the bands indicated above. The real part of ε behaves mainly as a classical oscillator. It vanishes (from positive to negative value) around 5.52, 10.01, 11.88, and 13.48 eV, and correspondingly, ε_2 shows the maxima of absorption at these frequencies. The real part ε vanishes (from negative to positive) at 6.40, 11.29, 12.72, and 14.96 eV (not seen in the figure because of the small broadening).

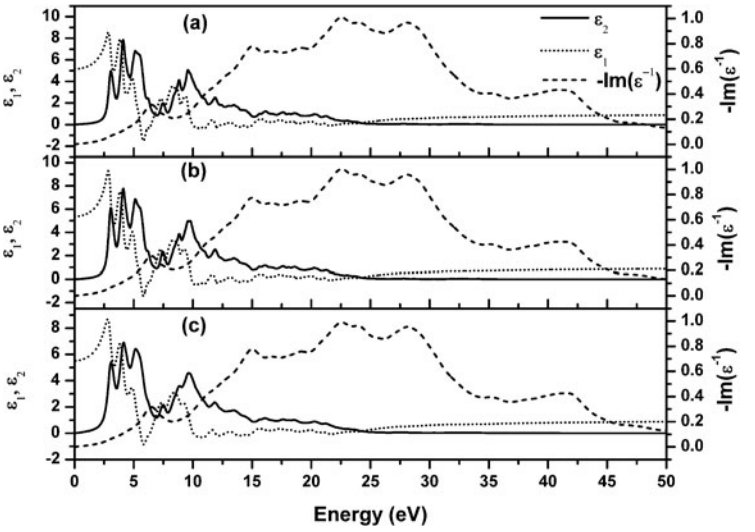

Figure 2. The calculated real (ε_1) and imaginary (ε_2) parts of the dielectric function and electron energy-loss spectra ($-\mathrm{Im}\varepsilon^{-1}$) of $KNbO_3$ in cubic (a), tetragonal (b) and rhombohedral (c) phases.

The loss function consequently shows peaks at these energies: 6.50 and 15.00 eV. In the absorption spectrum ε_2 the strong absorption below 8.0 eV stems from transitions from the valance band to the e_g states. The absorption band expending beyond 8.5 eV up to 14.0 eV is associated with transitions from the valence band to t_{2g} states in the conduction band. Second, we see that above 15.0 eV, corresponding to the O 2*s* and Nb 4*p* excitations, ε_1 also behaves as a classical oscillator: it vanishes (from positive to negative) at 21.30 eV. Peaks are observed in the loss function when ε_1 vanishes (from negative to positive) at 22.11 eV. Third, we remark that the region above 22.0 eV cannot be interpreted in terms of classical oscillators. Above 22.0 eV ε_1 and ε_2 are dominated by linear features, increasing for ε_1 and decreasing for ε_2. The corresponding loss function exhibits a broadened peak at 41.3 eV that we assign not to plasmons but rather to their forms of collective excitations. The plasmons are defined by a vanishing real part of dielectric function and a minimum of the imaginary part, which is not the case for this peak. Such linear behavior for ε_1 and ε_2 has already been observed in the theoretical EEL spectra of ABO_3. At higher energies, however, they drastically modify the triple 4*p* plasmons, both in line shape and peak position. We also find a small anisotropy for the *xx* and *zz* directions.

Conclusion

We have performed an ab initio study of the electronic structures of $KNbO_3$. Within the DFT-LDA framework, we have found it necessary to include the semicore states in the calculations. We have then followed the effect on the electronic structure as the crystal field evolves from a cubic to a tetragonal structure, and then to a rhombohedral. We have described a fingerprint in the electronic structure of cubic and rhombohedral $KNbO_3$. By using our earlier EEL spectroscopy experimental results on ABO_3 ferroelectrics and the theoretical investigation in the present paper, we found plasmon oscillation energy for the investigated compounds.

References

1. H. Ibach and D. L. Mills, *Electron Energy Loss Spectroscopy and Surface Vibrations*. N.Y: Academic Press, 1982.
2. P. E Batson, Electron Energy Loss Studies in Semiconductors, in: *Transmission Electron Energy Loss Spectrometry in Material Science and the EELS*. Weinheim: Wiley,-VCH Verlag, 2004.
3. M. Dressel and G. Grüner, *Electrodynamics of Solids: Optical Properties of Electrons in Matter*. Cambridge: Cambridge University Press, 2003.
4. X. Gonze, J. M. Beuken, R. Caracas, F. Detraux, M. Fuchs, G. M. Rignanese, L. Sindic, M. Verstraete, G. Zerah, F. Jollet, M. Torrent, A. Roy, M. Mikami, Ph Ghosez, J. Y. Raty, and D. C. Allan, First-principles computation of material properties: the ABINIT software project. *Comput Mater Sci*. **25**, 478–492 (2002).
5. X. Gonze, B. Amadon, P. M. Anglade, J. M. Beuken, F. Bottin, P. Boulanger, F. Bruneval, D. Caliste, R. Caracas, M. Cote, T. Deutsch, L. Genovese, P. H. Ghosez, M. Giantomassi, S. Goedecker, D. R. Hamann, P. Hermet, F. Jollet, G. Jomard, S. Leroux, M. Mancini, S. Mazevet, M. J. T. Oliveira, G. Onida, Y. Pouillon, T. Rangel, G. M. Rignanese, D. Sangalli, R. Shaltaf, M. Torrent, M. J. Verstraete, G. Zerah, and J. W. Zwanziger, ABINIT: First-principles approach to material and nanosystem properties. *Comput Phys Comm*. **180**, 2582–2615 (2009).
6. N. Troullier and J. L. Martins, Efficient pseudopotentials for plane-wave calculations. *Phys Rev B*. **43**, 1993–2006 (1991).
7. J. P. Perdew and Y Wang, Accurate and simple analytic representation of the electron-gas correlation energy. *Phys Rev B*. **45**, 13244–13249 (1992).
8. D. M. Ceperley and B. J. Alder, Ground state of the electron gas by a stochastic method. *Phys Rev Lett*. **45**, 566–569 (1980).
9. H. J. Monchorst and J. D. Pack, Special points for Brillouin-zone integrations. *Phys Rev B*. **13**, 5188–5192 (1976).
10. K. Rabe, C. H. Ahn, and J. M. Triscone, *Physics of Ferroelecrics: A Modern Perspective*. Heidelberg: Springer, 2007.
11. V. Gopalan, K. L. Schepler, V. Dierolf, and I. Biaggio, Ferroelectric Materials, in: *The Handbook of Photonics*. CRC Press Boca Baton, 2007.
12. A. M. Mamedov, Optical properties (VUV Region) of ABO_3 ferroelectrics: Application of syncrotron radiation. *Ferroelectrics*. **303**, 141–143 (2004). Mamedov AM: The Energy loss spectrum in oxygen –Octahedron. Ferroelectrics. **3,** 75–80(1985).
13. S. Cabuk, H. Akkus, and A. M. Mamedov, Electronic and optical properties of $KTaO_3$: Ab initio calculation. *Phys B*. **394**, 81–85. (2007).
14. S. Cabuk and S. Simsek, First-principles calculation of the lineer and nonlinear optical properties of $LiTaO_3$. *Phys Scr.* **81**, 055703–055711 (2010).
15. A. M. Mamedov, Vacuum ultraviolet (VUV) reflectivity and electron states in $LiNbO_3$. *Phys (B+C)*. **128**, 61–68 (1985).
16. A. M. Mamedov, M. A. Osman, and L. C. Hajieva, VUV reflectivity of $LiNbO_3$ and $LiTaO_3$ single crystals. *Appl Phys A*. **34**, 189–192. (1984).
17. E. E. Krasovskii, O. V. Krasovskii, and W. Schattke, Ab initio calculation of the optical and photoelectron spectra of $KNbO_3$ and $KTaO_3$. *J Electron Spectr Rel Phen*. **83**, 121–127 (1997).
18. C. M. I. Okoye, Theoretical study of the electronic structure, chemical bonding and optical properties of $KNbO_3$ in the paraelectric cubic phase. *J Phys: Cond Matter*. **15**, 5945–5959 (2003).
19. H. Wang, F. Wu, and H. Jiaug, Electronic band structures of $ATaO_3$(A = Li, Na, and K) from first-principles many-body perturbation theory. *J Phys Chem C*. **115**, 16180–16186 (2011).
20. Y. Shiozaki, E. Nakamura, and T. Mitsui, *The Landolt-Bornstein Database*. Berlin: Springer New Ser. III/36, 2002.